AIMS Geosciences

AIMS Geosciences, 6(4): 545–560.
DOI: 10.3934/geosci.2020031
Received: 15 October 2020
Accepted: 08 December 2020
Published: 16 December 2020

http://www.aimspress.com/journal/geosciences

Research article

Response of IAR frequency scale to solar and geomagnetic activity in solar cycle 24

Alexander S. Potapov* and Tatyana N. Polyushkina

Institute of Solar-Terrestrial Physics SB RAS, Irkutsk, Russia

*** Correspondence:** Email: potapov@iszf.irk.ru.

Abstract: The ionospheric Alfvén resonator (IAR) is an integral element of the entire ionosphere-magnetosphere system. It plays an essential role in energy exchange and interaction between the magnetosphere and ionosphere. The parameters of this resonator reflect the state of the ionosphere. The purpose of this study was to study three types of IAR frequency modulation (daily, seasonal and solar-cyclic) and to identify their relationship with solar and magnetic activity. We used the results of magnetic observations of the IAR emission at the Mondy mid-latitude observatory for the 24th solar activity cycle from 2009 to 2019. The dependence of the difference in the neighboring harmonics frequencies (i.e., the emission frequency scale) on solar activity (the sunspot number) and on the magnetic indices Kp, Dst and AE was studied. The correlation between the frequency scale and the indices of solar and magnetic activity was investigated at different time scales by comparing the variations in daily, monthly, and annual averages. The dependence of the IAR frequency scale on solar activity turns out to be much closer than the same dependence of any of the three magnetic indices. The closest relationship is exhibited between the annual average values of the frequency scale, on the one hand, and the sunspot number and the Dst index, on the other. This result is interpreted as a demonstration of the cumulative effect of solar activity on the state of the ionosphere and, first of all, on the electron concentration in the F2 region of the ionosphere.

Keywords: resonator; frequency modulation; ULF emissions; spectrogram; resonance harmonics

1. Introduction

The complex structure of the magnetospheric-ionospheric dynamic system includes a whole set of waveguides and resonators. The most well-known of them are the field-line resonator [1,2], an

ionospheric waveguide [3], an earth-ionosphere resonator [4], a waveguide under the roof of the plasmasphere [5]. In the last quarter of the previous century, an ionospheric Alfvén resonator (IAR) was predicted [6] and discovered [7]. IAR is a cavity between the base of the ionosphere and the region of transition to the magnetosphere.

The lower boundary of the cavity is a sharp gradient of Alfvén velocity $V_A = B/(4\pi\rho)^{1/2}$ at a level of about 100–150 km, which arises due to the fact that the magnetic field B decreases with altitude much more slowly than the increase in the density of charged particles ρ, which reaches a maximum in the F2 region of the ionosphere (250–350 km). Above this layer, the plasma density decreases, although somewhat more slowly than it increases; and at an altitude of about 1000 to 6000 km, a maximum of the Alfvén velocity forms, which serves as the upper boundary of the cavity. (The specific altitude value depends on the state of the magnetosphere-ionospheric system). The frequency of Alfvén waves trapped in the cavity lies in the upper part of the range of ultra-low-frequency (ULF) electromagnetic oscillations, below 10 Hz. On the daily spectrogram of magnetic oscillations, IAR emission has the characteristic form of discrete spectral bands, their frequency and the distance between them (frequency scale) increase from noon to midnight and decrease in the morning hours. A typical example of a dynamic emission spectrum is shown in Figure 1.

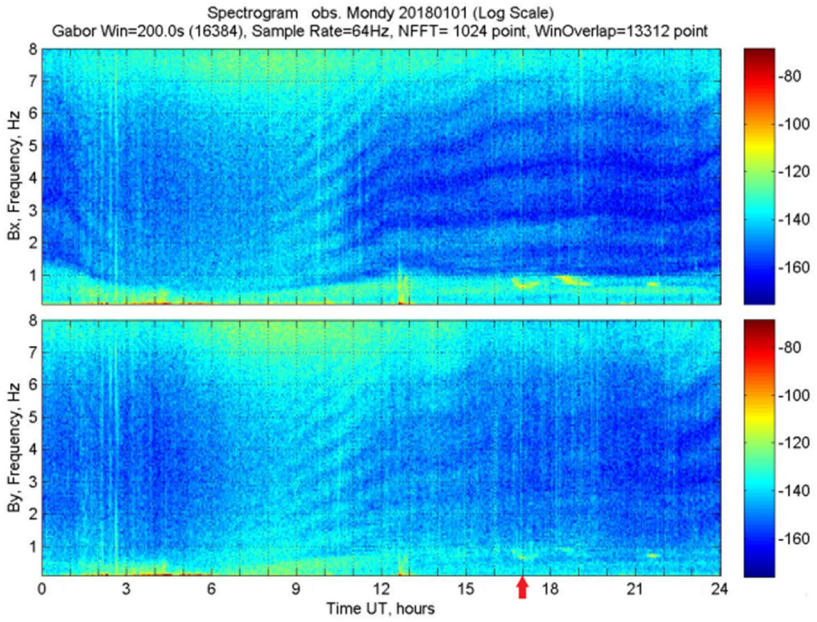

Figure 1. An example of a daily IAR emission spectrogram. Two components of the magnetic field are shown: meridional (B_x) and azimuthal (B_y). The colored bars on the right allow one to correlate the colors in the dynamic spectrum with the emission intensity in decibels. The arrow below the time axis shows local midnight.

Subsequently, IAR was actively studied by the joint efforts of many authors. The main contribution at the first stage of research was made by works [8–10]. The discoverers of the IAR developed the theory of the emission spectral structure [8]. The presence of the ionospheric Alfvén resonator was shown to give rise to a rapid accumulation of energy in the upper ionosphere [9]. A theory was proposed of feedback interactions which are controlled by reflections within the IAR

resonant cavity [10]. Following these studies, a stream of publications emerged in the literature. Various theoretical models of IAR were proposed (see, for example, the review [11] and references therein) and the results of observations of IAR emission in various regions were analyzed [12–20]. By now it has become clear that the ionospheric Alfvén resonator is an integral element of the entire ionospheric-magnetospheric structure. It plays an essential role in energy exchange and interaction between these two regions of near-Earth space.

The published works contain a fairly complete morphological description of the IAR emission; they also include an analysis of the relationship between the emission characteristics and other geophysical phenomena. In particular, the close relationship between the harmonic frequency set of the emission and the critical radio sounding frequency f_0F2 of the F2 region of the ionosphere was measured, analyzed in detail and explained [13,15,17,21–23]. (The fact is that the resonance frequencies of the IAR depend primarily on the concentration of electrons N_e in the ionosphere and the frequency f_0F2 is rigidly connected with this concentration: $N_e = 1.24 \times 10^4 (f_0F2)^2$, here N_e is measured in particles per cubic centimeter, and the critical frequency is in megahertz.) However, all the above-mentioned works used observational data for a limited time interval, and the equipment used was not always sufficiently sensitive and noise-immune to be able to register the IAR emission on any day, regardless of the season and phase of the solar cycle. This hinders the successful study of such an important object for the physics of the ionosphere-magnetosphere system as the ionospheric Alfvén resonator. The properties of its emission contain a response to the processes of interaction between the ionosphere and magnetosphere. It can be expected that the data from measurements of the IAR harmonic structure will eventually serve as an additional tool for studying the upper atmosphere, just as in recent decades the measurement of total electron content using satellites of global navigation systems has become such an instrument.

The aim of this work was to study three types of IAR frequency changes during the solar cycle: daily, seasonal, and solar-cyclic frequency modulation. The task was to reveal, on this basis, the dependence of the emission frequency on solar and geomagnetic activity on all three time scales.

2. Methods for measurement and preliminary analysis

Discrete spectral bands in Figure 1 reflect the harmonic structure of the emission. The entire emission range occupies the interval from tenths of a hertz to about 8 Hz that is the frequency of the first harmonic of the Schumann resonance. But sometimes the frequency range of the IAR goes beyond 8 Hz. The emission amplitude is small; it does not exceed several picotesla. In fact, we see noise, the intensity of which is modulated by the resonator. Frequencies close to the resonance frequencies of the IAR are distinguished from the continuous spectrum of the noise background. In contrast to the Schumann resonances (the first harmonic of which is visible as a horizontal band at the upper edge of the spectrogram, Figure 1), the frequency of each of the IAR harmonics changes continuously throughout the day, passing two or three octaves. The fact is that Schumann resonances arise in a global spherical earth-ionosphere resonator, the parameters of which almost do not change over time. In contrast, the resonance frequencies of the IAR are determined mainly by the electron concentration in the ionosphere, which varies greatly during the day in accordance with changes in the ultraviolet radiation flux from the Sun.

The low amplitude of the IAR emission requires the use of highly sensitive equipment for its measurement and the absence of external interference of artificial or natural origin. The most

commonly used device for recording ULF emission of this kind is an induction magnetometer. It consists of a multi-turn coil with a high permeability alloy core, a preamplifier, a set of filters, an analog-to-digital converter (ADC), and a digital storage device. In this work, we used the observation data from a mid-latitude magnetic station located far from sources of industrial interference on the territory of the Mondy Solar Observatory. Geographic coordinates of the Obs. Mondy are 51.62°N, 100.91°E, corrected geomagnetic coordinates are 47.48°, 174.86° (epoch 2015). Magnetic station is equipped with a highly sensitive induction magnetometer LEMI-30 [24]. This magnetometer has a magnetic noise level of less than 0.2 $pT \cdot Hz^{-1/2}$ at 1 Hz. For timing, the device is equipped with a signal receiver from the global navigation satellite system. Two horizontal components of ULF oscillations of the magnetic field were recorded. The magnetometer was located away from sources of industrial noise and included a 24-bit ADC with a 64 Hz sampling rate and a 50 Hz notch filter. The observations were carried out almost continuously throughout the entire solar cycle 24. This made it possible to collect material that allows one to confidently analyze a variety of emission characteristics based on a long series of high-quality measurements.

The observation period lasted from October 2009 to June 2019. Of all the data for this 3195 day period, data for 2509 days were suitable for processing; the remaining 686 days the equipment did not work for various reasons. The primary processing consisted in constructing the daily dynamic spectra of the output signal from the magnetometer in the range of 0–8 Hz, see Figure 1. Preliminarily, the most suitable values of the spectral window, overlap and other parameters were selected, consistent with the parameters of the ADC used. Of the 2509 spectrograms obtained, 2444 contained at least small portions of the spectral bands of the IAR emission. For further processing, we selected days with clear spectral bands around local midnight (17 UT). There were 1442 such spectrograms.

Further analysis was carried out by visual methods: the frequency values of each of the spectral bands at certain points in time were measured on the spectrogram using a cursor. Details of the processing method can be found in [19,22]. For the purposes of this study, we measured the band frequencies corresponding to local midnight, since it is at this time that the maximum development of the phenomenon can be expected. The frequencies of the harmonics (bands) of the emission approach the maximum values at local midnight. Then, for each moment in time, the frequency difference averaged over the observed bands was calculated as an estimate of the frequency scale Δf of the resonator. For a limited observation interval, the band frequencies were also measured at 11 UT (18 LT—dusk) and 23 UT (06 LT—dawn). The data obtained were entered into tables, which were compared with similar tables of other geophysical parameters; monthly and annual average values were calculated, and statistical and other types of analysis were carried out. Details will be provided in the following sections.

The solar cycle is an approximately 11-year change in the Sun's activity measured usually in terms of sunspots number or 10.7 cm radio flux intensity. At the minimum between two cycles, the large-scale dipolar magnetic field of the Sun reverses its polarity. See [25] for details. The 24th cycle of solar activity (Figure 2), within which the data of our observations lie, began in December 2008 and ended according to preliminary data [26] in December 2019. Thus, the observation period analyzed here (October 2009–June 2019) is only 14 months shorter than the total 132-month duration of the solar cycle 24. The ascending phase of the cycle took about two years from mid-2009 to mid-2011. The double high of the cycle lasted from mid-2011 to the end of 2014. Finally, the decay phase took the remaining 4 years—from 2015 to 2018. Years 2009 and 2019 may be referred as years of the minima between solar cycles 23 and 24, and between cycles 24 and 25, respectively. Over the entire

cycle, there were 48 X-class solar flares. Overall, this was the weakest cycle since the Dalton minimum [27] of solar activity in 1790–1830. Data on sunspot numbers are collected by the World Data Center WDC-SILSO, Royal Observatory of Belgium, Brussels [28] and available from the OMNIWeb website [29].

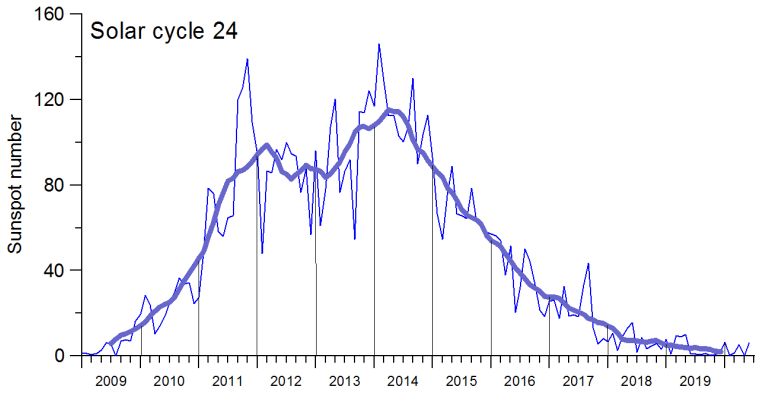

Figure 2. Variation in the number of sunspots during the solar cycle 24. Thin broken line shows mean monthly values of sunspot numbers. The solid thick line is a 13-point moving average.

There is no single index that would describe all aspects of geomagnetic activity. So we used three geomagnetic indices: Kp, AE, and Dst. Kp index characterizes geomagnetic activity averaged over the whole planet and is calculated from measurements of magnetic stations in a wide range of latitudes. This index is available from FTP server of the GFZ German Research Centre for Geosciences [30] and from the OMNIWeb website [29]. AE index describes the auroral activity associated with the intensity of auroral electrojets, it increases during the development of substorm and storm disturbances. Dst index shows the intensity of the ring current, which intensifies during magnetospheric storms. Both AE and Dst indices are available from the Kyoto University World Data Center for Geomagnetism [31] and from the OMNIWeb website [29].

3. Results

Figure 3, which shows the time variation of monthly average values of the frequency scale Δf for the entire observation period, clearly indicates that, in addition to the daily frequency modulation, which is clearly visible in the spectrogram in Figure 1, IAR emission is also subject to seasonal and solar-cyclic modulation.

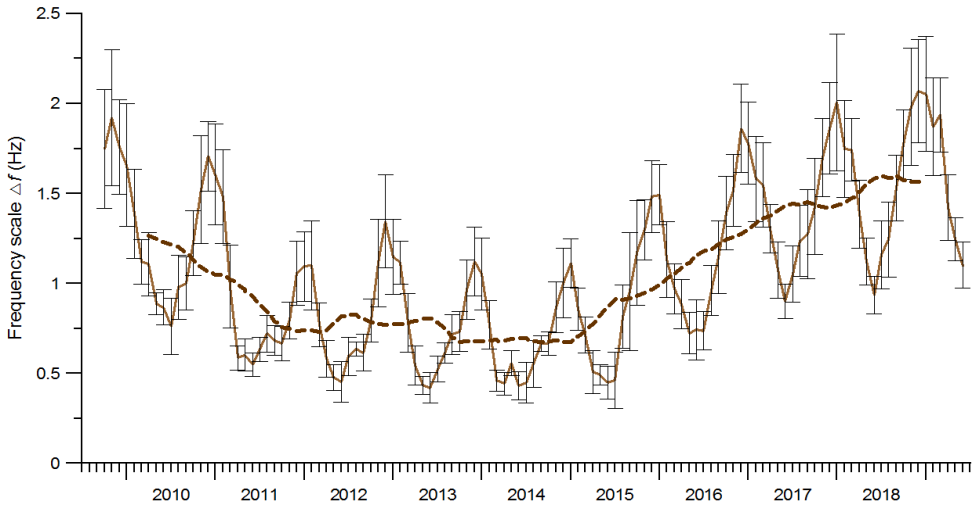

Figure 3. Variations in monthly mean values of Δf over an almost 11-year observation period. Vertical lines show the standard deviations of the calculated values of Δf; the dashed line is a 13-point moving average.

The minimum of the averaged cyclical variation of the frequency scale (starting from the second half of 2013 and including the entire 2014) exactly coincides with the phase of the maximum of solar cycle 24, and the maxima of Δf values are reached in the year of the cycle minimum (2009 and 2019). The peak of the seasonal variation of Δf corresponds to the winter months, and the minimum to the summer months. Further, we will consider in more detail all three periods of modulation of the frequency scale of the IAR emission and their relationship with variations in solar and magnetic activity.

3.1. Daily and seasonal modulation

The daily modulation of both the IAR resonance frequencies and the frequency scale Δf of the emission was studied in detail in previous works [13,15,21–23,32]. In [17,18,33] this dependence was modeled basing on the ionosphere parameters reconstructed from the IRI model. The resonance frequencies and their difference are inversely proportional to the square root of the electron concentration N_e in the F2 region of the ionosphere, since these frequencies are determined primarily by the value of the Alfvén velocity in the region of the minimum of its altitude profile, which coincides with the F2 layer. The same conclusion explains the inverse dependence of the above frequencies on the critical frequency f_0F2, since $f_0\text{F2}\sim(N_e)^{1/2}$. The correlation between these values is very high: the linear correlation coefficient between the hourly values of $(\Delta f)^{-1}$ and f_0F2 usually does not fall below 0.8.

Here we will pay attention to the depth of the daily modulation of the IAR emission frequency and its possible dependence on solar and magnetic activity. As one can see in Figure 1, the entire "comb" of spectral bands shifts up and down during the day, from the minimum values of the frequency of all bands and the distance Δf between them near the local noon, to the maximum values at midnight or early morning hours. From day to day and depending on the season, the position of the frequency extremes may shift in one direction or the other by one or two hours. The frequency modulation depth also changes. It can be measured relatively accurately only in the winter months, since the rest of the time, especially with moderate and high solar activity, the spectral bands are weakly expressed or not

observed at all in the daytime, when the ionosphere is illuminated over the observation station [17]. The difference between the Δf values at midnight (0 LT) and evening (18 LT) relative to the midnight Δf value can give a rough indication of the depth of frequency modulation. (The relationship between midnight and evening values of Δf and the regression relationship between them are shown in Figure 4a.) We tracked changes in the frequency modulation depth throughout the observation period. The result is presented in Figure 4b, which shows the monthly averages of κ_{mod} calculated from $\Delta f_{midnight}$ and Δf_{dusk} measured on individual days of a month $\kappa_{\text{mod}} = (\Delta f_{midnight} - \Delta f_{dusk}) / \Delta f_{midnight}$, the solid broken line shows variations of the κ_{mod} indicator of the depth of the daily frequency modulation; the dashed line segments show the areas where κ_{mod} could not be estimated. Only those months were taken for which $\Delta f_{midnight}$ and Δf_{dusk} measurements were available for three or more days. Error bars show standard deviation of averages. It can be seen that at the ascending phase of the solar activity cycle (2010–2012), a fairly regular seasonal variation in the depth of diurnal modulation is observed. At the peak of activity since the second half of 2013, this regularity is disrupted. It recovers only in 2016, a year and a half after the start of the decay phase, and continues until the end of the cycle. There are very significant changes in the modulation depth: from 0.25–0.4 in the winter months to 0.7–0.75 in the spring-summer and autumn.

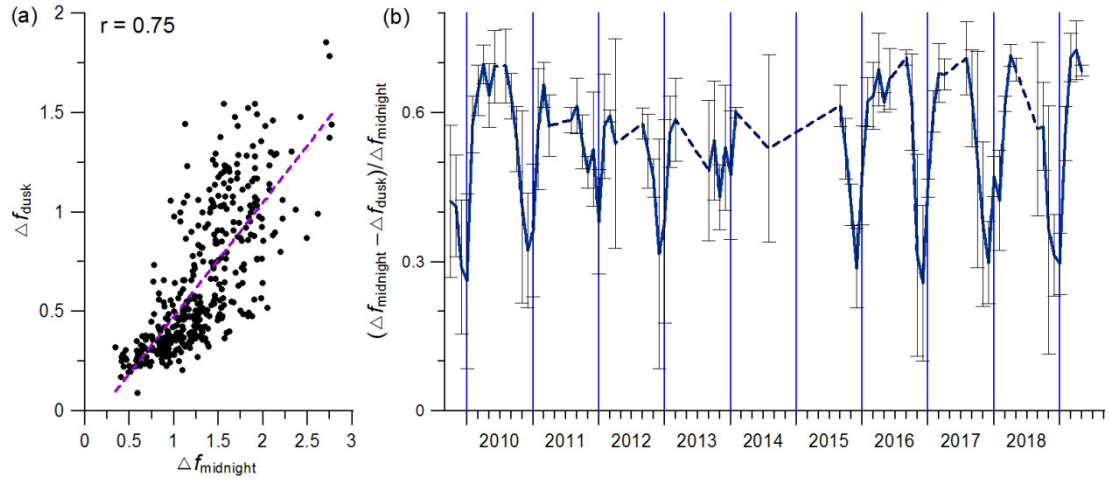

Figure 4. (a) Ratio between evening and midnight values of Δf; the dashed line shows the regression. (b) Changes in the depth of Δf daily modulation for the entire observation period; solid line shows changes in the κ_{mod} parameter; dashed line segments mean no data.

The depth of the daily modulation of the IAR frequency scale weakly depends on the geomagnetic activity. The largest linear correlation coefficient $r = 0.44$ was obtained between the monthly mean values of κ_{mod} and auroral activity, characterized by the AE index. Increasing the AE increases the modulation depth slightly. Variations in the monthly mean number of sunspots W have no effect on the course of the monthly mean values of κ_{mod}.

The reason for the seasonal variation in the frequency of the IAR emission is, as in the case of the diurnal variation, the seasonal variation in the electron concentration in the F2 region of the ionosphere. Judging by Figure 3, in the solar activity cycle, the seasonal frequency modulation, as well as the variation in the depth of diurnal modulation, is most pronounced at the growth and decline phases of the cycle.

Figure 5 shows the cycle-averaged seasonal variation of the frequency scale of the IAR emission. To plot the graph, the average value $\Sigma_i(\Delta f_{ij})/12$ for the corresponding j-th year was subtracted from each monthly average value Δf_{ij}, after which the cycle-averaged S_i values of the seasonal frequency-scale variation were calculated (this procedure has excluded the cyclical variation of Δf):

$$S_i = \sum_j \left(\Delta f_{ij} - \sum_i (\Delta f_{ij})/12 \right) \Big/ 9, \quad (1)$$

here Δf_{ij} means the average for the i-th month of the j-th year value of the frequency scale Δf, calculated from the measurements of harmonic frequencies at midnight local time (17 UT); i = 1, 2, ..., 12; j = 1, 2,…, 9. We used the measurement results for 9 full years, from 2010 to 2018.

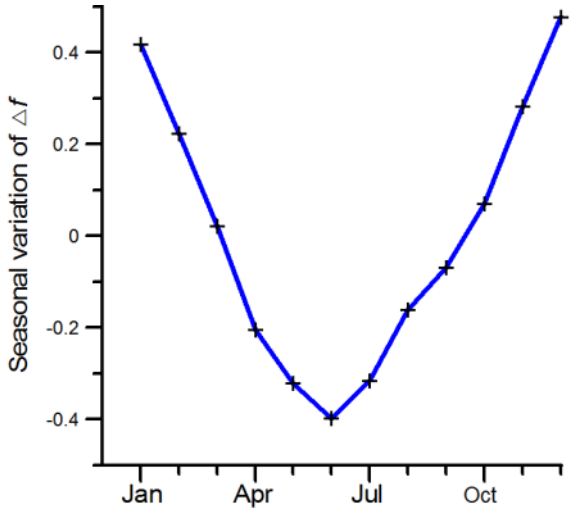

Figure 5. Cycle-averaged seasonal modulation of the IAR emission frequency scale.

3.2. Dependence on solar and magnetic activity

Now we consider the relationship between the frequency structure of the IAR emission and the indices of magnetic and solar activity at different levels of averaging of the compared parameters. The Δf values measured at local midnight (17 UT) will be used as the daily values of the IAR frequency, which will be compared with the simultaneous (in universal time) daily values of the magnetic indices Kp, Dst, and AE. As monthly averages of the frequency scale Δf and magnetic indices, we used averages calculated for the days of each month when Δf measurements were available. We calculated the monthly averaged sunspot numbers and geomagnetic indices by averaging them over the same days that we used to average Δf. Finally, the IAR frequency-scale and geomagnetic indices annual averages were calculated by simple yearly averaging of the obtained monthly values. The annual averages of solar activity are taken from the OMNI website [29]. All annual averages are presented in Table 1.

Table 1. List of the annual averages of parameters used in the analysis.

	2009*	2010	2011	2012	2013	2014	2015	2016	2017	2018	2019*
Δf	1.81	1.19	0.86	0.80	0.76	0.66	0.86	1.13	1.40	1.56	1.61
W	10.3	24.9	80.76	84.39	93.71	113.6	69.78	39.82	21.88	7.08	6.42
Dst	0.77	−10.51	−12.47	−10.47	−11.62	−10.86	−10.49	−8.92	−9.31	−5.00	−5.09
AE	39	125	146	169	159	149	190	189	178	98	---
Kp	5.37	13.5	15.5	16.5	14.9	16.1	19.0	18.8	18.0	14.1	13.8

* Averages for these years were calculated by averaging monthly values over a part of the year (see text).

We start with the daily averaging scale. Figure 6a shows scatter plots of simultaneous measurements of Δf and geomagnetic indices Dst and AE. Both plots show a triangular shape of the point cloud. The connection between Δf and indices Dst and AE is weak, but the plots show clearly that the highest values of Δf are observed at the lowest geomagnetic activity (AE ≤ 200 and Dst ≥ –30), i.e., in the magnetically quiet times. And, conversely, at the highest activity (AE ≥ 500 and Dst ≤ –40), we see only low values of the frequency scale Δf. To assess the reliability of the dependence of the IAR frequency structure on the magnetic activity, we divided the entire array of hourly data into quartiles according to the AE values and plotted the Δf distributions for each quartile. The distributions for the first and fourth quartiles are shown in Figure 6b on the top and bottom panels, respectively. It can be seen that the distribution for the fourth quartile is shifted relative to the first one towards larger values of Δf. The difference in the position of the distribution maxima is 0.35 Hz, which, however, is less than the standard deviation in determining the position of the maxima (0.42 Hz). Thus, we can only speak about the tendency of the dependence of Δf on AE. The connection between Δf and Dst and Kp turned out to be even weaker.

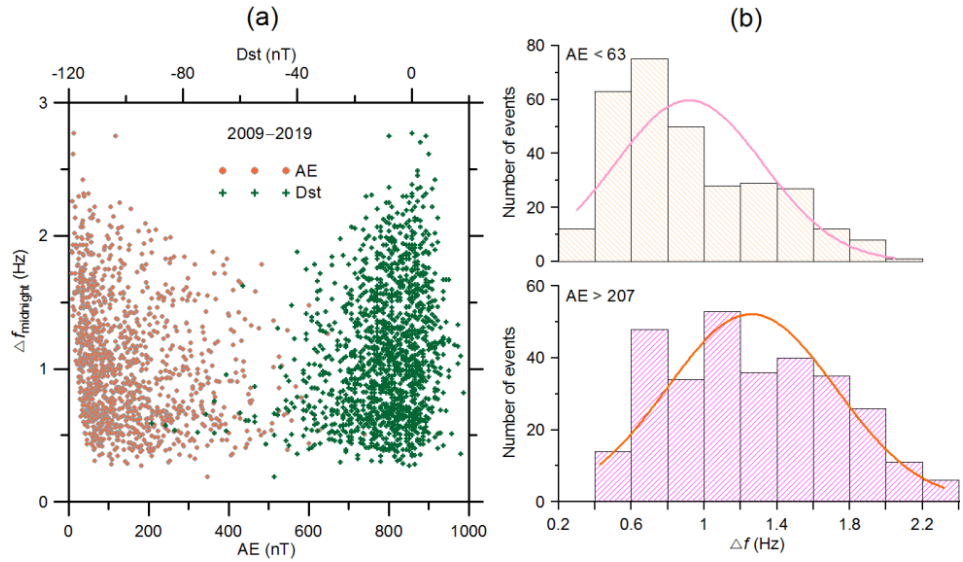

Figure 6. (a) Scatter plots of simultaneous daily measurements of Δf and geomagnetic indices AE and Dst; (b) Histograms of Δf distributions for the first quartile of AE index (quiet conditions, upper panel) and the fourth quartile (high-disturbed conditions, bottom panel). Solid lines show Gauss fitting of the distributions.

At the level of monthly average values, the relationship between Δf and magnetic activity becomes more obvious, although it remains only a trend. The linear correlation coefficients between the monthly averages Δf and the magnetic indices for the entire sample of 117 months are 0.38 for AE, 0.35 for Dst, and 0.27 for Kp.

The relationship between the inverse value of the monthly average frequency scale Δf and the monthly sunspot number looks more convincing exhibiting a correlation coefficient $r = 0.66$, Figure 7a. It turns out to be closer than the relationship between the monthly average Dst index and the sunspot number ($r = 0.29$), Figure 7b. The correlation of the monthly mean Kp and AE with solar activity is even weaker (0.09 and 0.04, respectively).

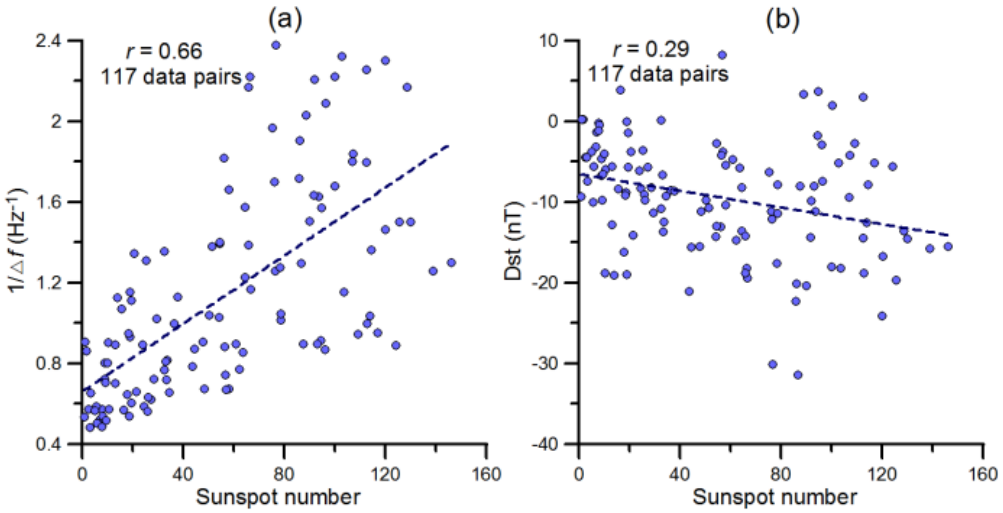

Figure 7. Scatter plot of (a) inverse monthly Δf averages and sunspot numbers; (b) monthly averages Dst and sunspot numbers.

One can finally be convinced of the significant influence of solar activity on the IAR frequency regime only by comparing the average annual values of the frequency scale and the sunspot number during the 11-year cycle. Figure 8a,b show the results of such a comparison. Two equal representations are given: $\Delta f^{-1}(W)$ and $\Delta f\,(W)$, where W is the average annual sunspot number. Regression relations are presented. In both concepts, the connection between the frequency scale of the IAR emission and the solar-cycle activity looks quite convincing, especially in comparison with the relationship between solar and magnetic activity, which is much weaker even on the time scale of the solar cycle. For comparison, Figure 8c shows the dependence of the average annual Dst index on the sunspot number; linear and logarithmic approximations are shown. This index has the closest connection with W compared to Kp and AE indices: for them, linear correlation coefficient is 0.41 and 0.5, respectively. Note that the calculation of averages Δf, W and Dst for 2009 and 2019 was carried out according to the data of the last 3 and first 6 months of the year, respectively.

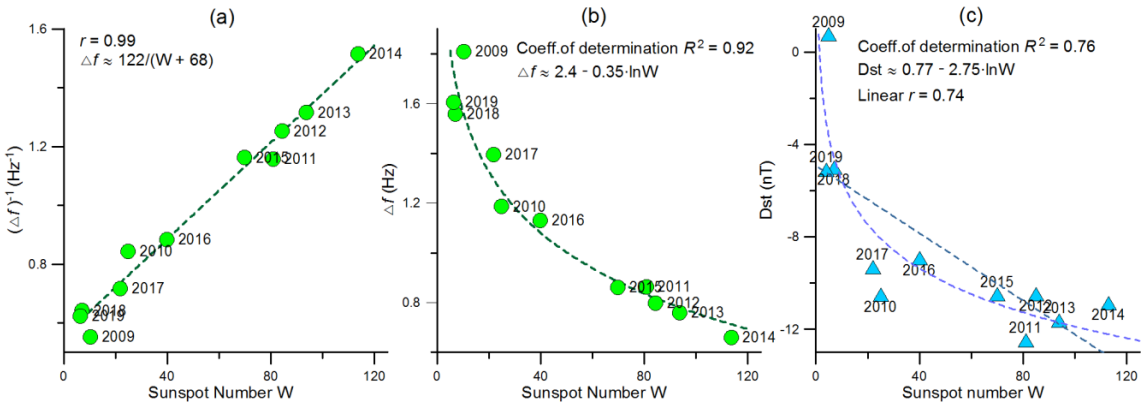

Figure 8. Scatter plots of (a) inverse frequency scale $1/\Delta f$ versus yearly averaged sunspot number W; (b) frequency scale Δf versus W; (c) yearly averaged Dst index versus W. Dashed lines are (a and c) linear regression and (b and c) logarithmic regression.

Now consider the dependence of the average annual values of the IAR frequency scale on magnetic activity (Figure 9a–c). The plots confirm once again that the Dst index is the most correlated with the IAR frequency; the coefficient of linear correlation of its mean annual values with Δf is 0.88 (Figure 9a). The correlation of the other two indices of magnetic activity, AE and Kp, is much weaker, their correlation coefficients do not exceed 0.7 (Figure 9b,c).

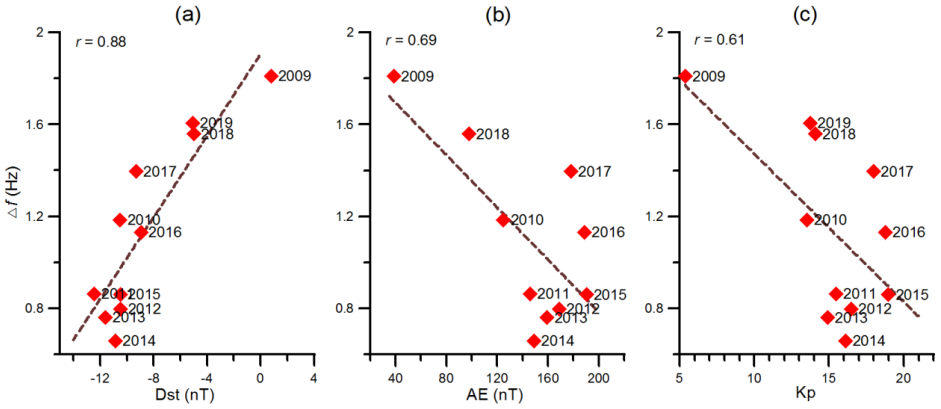

Figure 9. Scatter plots of (a) frequency scale Δf versus yearly averaged Dst index; (b) frequency scale Δf versus yearly averaged AE index; (c) frequency scale Δf versus yearly averaged Kp index. Dashed lines are linear regression between analyzed parameters.

4. Discussion

We have shown that the frequency resonance structure of IAR emission, characterized by its frequency scale (distance Δf between adjacent harmonics), changes significantly in the solar activity cycle. These changes and their relationship with solar activity are most clearly manifested in the cyclical variation of the mean annual values of Δf and their dependence on the number of sunspots. At shorter time scales, this relationship is much less pronounced. In our opinion, this indicates the inertia of the processes of solar radiation impact on the Earth's ionosphere. Long-term changes in the electron

concentration, the height of its maximum, and the ionic composition, in addition to the response to the daily and seasonal changes in X-ray and ultraviolet radiation, accumulate changes associated with the total solar activity in the cycle. This is the cumulative effect of solar activity. At the same time, shorter-period variations in the number of sunspots from month to month, being almost unrelated to variations in short-wave radiation, have little effect on the state of the ionosphere and weakly correlate with the IAR frequency regime.

As for the magnetic activity, of the three considered indices, only Dst has a noticeable correlation with both the number of sunspots (Figure 8c) and the frequency structure of the IAR (Figure 9a), but only on the time scale of the solar cycle. This index is closely related to solar flares that cause magnetic storms and amplification of the ring current, the intensity of which is measured by Dst. The number of flares has a distinct cyclical course. It is possible that we were unable to identify the actual effect of the solar flare activity on the IAR regime on a shorter time scale due to the fact that we used the averaged values of the Dst index, and not the minimum ones, which are directly related to magnetic storms, as echoes of flares. Similar considerations apply to the other two magnetic activity indices. Averaging can smooth out and even hide the influence of magnetic disturbances, which we have no doubt about: it was demonstrated in [23,34]. In addition, since we used mid-latitude observatory data, the influence of the auroral AE index could not be very noticeable.

Looking at Figure 9 one can notice that the points on all of three plots are distributed unevenly: points presented years of higher activity are grouped in the bottom left or right corner. We checked the correlation between Δf and Dst, AE, Kp separately during higher and lower solar activity. The results are presented in Table 2. Linear correlation coefficient during minimum and declining phases (2009–2010 and 2016–2019) turned out to be much higher than during period of high solar activity (2011–2015). So we have two different regimes of connection between IAR frequency and geomagnetic activity. Probably this fact reflects different mechanisms of solar action on the ionosphere.

Table 2. Linear correlation coefficients between Δf and geomagnetic indices during periods of high and low solar activity.

Solar activity	Kp	AE	Dst
High (2011–2015)	0.38	0.43	0.24
Low (2009–2010 and 2016–2019)	0.80	0.84	0.92

It is known that one of the noticeable effects of the solar cycle on the ionosphere is a change in the ionic composition, especially in the upper regions of the ionosphere. Possibly, this can serve as an additional factor (in addition to changes in the electron density), leading to the observed cyclic variation of the frequency of the IAR emission. Indeed, the ionic composition and its height profile significantly affect the Alfvén velocity profile along the axis of the resonator and, consequently, the resonant frequencies. Earlier it was even proposed to diagnose the relative abundance of ions by measuring the frequency structure of the IAR. In [8], the possibility of such a diagnosis was substantiated, and in [35], a practical attempt was made to estimate the altitude profile of the ionic composition from measurements of the IAR emission. The authors used magnetic observations made during the epoch of minimum solar activity at mid-latitude and auroral stations. Profiles of the relative abundances of hydrogen, oxygen and helium ions were obtained. It would be useful to repeat these estimates for other phases of the solar cycle.

It should be noted that the IAR emission depends on the state of the ionosphere in a more complex way than, for example, the critical frequency f_0F2 of ionospheric radio sounding. The latter, as noted, is rigidly related to the electron concentration N_e in the F2 region, being proportional to the square root of the electron density at the maximum of the height profile N_e. It does not depend on any other ionospheric parameters. On the contrary, for the IAR frequency scale, the electron concentration is only the main determining parameter, but the value of Δf is also influenced by the form of the height profiles of N_e, the ionic composition, and the intensity of the geomagnetic field, since all these parameters determine the conditions for the propagation of Alfvén waves along the axis of the resonator.

A striking example of the absence of a continuous correspondence between the variations $1/\Delta f$ and f_0F2 is Figure 10, which shows the simultaneous changes in the monthly mean values of these parameters from March 2010 to May 2011.The figure shows that if in the interval from September 2010 to May 2011 two parameters change in general in agreement, then before that, from March to September 2010, they vary out of phase. As previously shown [19], although within one day the relationship between $1/\Delta f$ and f_0F2 is usually close (the correlation coefficient does not fall below 0.8), but on different days this relationship, while remaining close, can significantly change their regression coefficients. This is precisely what can lead to the fact that the variations of the monthly mean values $1/\Delta f$ and f_0F2 can differ significantly.

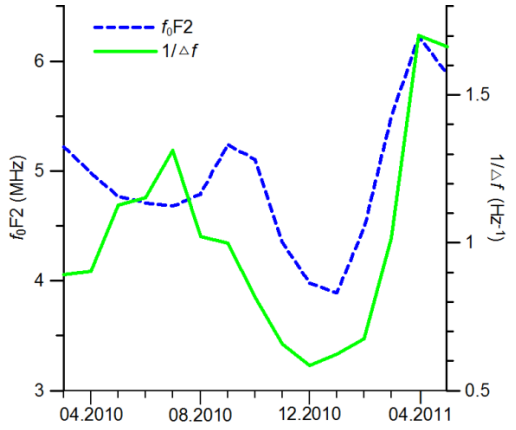

Figure 10. An example of simultaneous variations of the monthly mean values of $1/\Delta f$ and f_0F2 from March 2010 to May 2011.The solid green line shows the variations of the reciprocal of the IAR frequency scale, and the dashed blue line shows the variations of the critical frequency f_0F2 of ionospheric radio sounding.

If one strives to obtain useful information about the state of the ionosphere from ground-based data by remote methods, then one should compare all the relationships considered in the article with similar dependences also for the critical frequency f_0F2 and the total electron content TEC. The authors leave this task for future research, since there have not yet appeared any works in the literature analyzing the behavior of f_0F2 and TEC for the 24th solar cycle. An exception is an interesting article [36] on the impact of solar flares of 23–24 cycles on TEC, but it includes only a small interval of the 24th cycle.

We have not touched here on other possible ways of indirect influence of solar activity on the radiation of IAR, for example, thunderstorm activity, which is considered the main source of energy for powering the IAR [37]. However, we should note that the main goal of this work was to reveal the

effects of periodic modulation of IAR emission and compare them with the modulation of solar and magnetic activity.

5. Conclusion

In this study, we used the results of magnetic observations of the IAR emission from the Mondy mid-latitude observatory for the period of the 24th solar activity cycle from 2009 to 2019 to reveal the dependence of the emission frequency scale on the sunspot number and the magnetic indices Kp, Dst and AE. Since it turned out that the emission frequency undergoes diurnal, seasonal, and cyclical variations, the degree of correlation between the frequency scale and the indices of solar and magnetic activity was studied at different time scales by comparing the variations in daily, monthly, and annual mean values. The dependence of the IAR frequency scale on solar activity is much closer than the same dependence of any of the three magnetic indices. The closest relationship was found between the average annual values of the frequency scale, on the one hand, and the number of sunspots and the Dst index, on the other.

The found regularities of the relationship between the frequency regime of the IAR and the solar and magnetic activity in the solar cycle can be used to refine the models of both the IAR itself and various ionospheric models. We hope that the results obtained here will contribute to understanding the mechanisms of the effect of solar radiation on the state of the ionosphere and the processes occurring in it. Moreover, we believe that over time, information on the IAR frequency structure obtained with induction magnetometers will be routinely used to monitor the state of the ionosphere, just as in the recent past TEC measurements with GPS signal receivers began to be used for this.

Acknowledgments

The authors are grateful to B. Tsegmed for help in processing the magnetic records. We are grateful to the administration of the OMNI website for providing open access to the archive of magnetic and solar activity indices.

This work was supported by the Russian Foundation for Basic Research (grant number 19-05-00574) and budget financing from the Ministry of Science and Higher Education of the Russian Federation (Program II.16). The results were obtained using the equipment of ANGARA Center of Common Use http://ckp-rf.ru/ckp/3056/.

Conflict of interest

All authors declare no conflicts of interest in this paper.

References

1. Hasegawa A, Chen L (1974) Theory of magnetic pulsations. *Space Sci Rev* 16: 347–359.
2. Southwood DJ (1974) Some features of field line resonances in the magnetosphere. *Planet Space Sci* 22: 483–491.
3. Greifinger C, Greifinger P (1968) Theory of hydromagnetic propagation in the ionospheric waveguide. *J Geophys Res* 73: 7473–7490.

4. Schumann WO (1952) On the radiation free self oscillations of a conducting sphere, which is surrounded by an air layer and an ionospheric shell. *Z Naturforsch* 72: 149–155.
5. Guglielmi AV (1979) *MHD Waves in Near-Earth Plasma*, Moscow Nauka Pbl, 1–139.
6. Polyakov SV (1976) On the properties of ionospheric Alfvén resonator, *Simpozium KAPG po solnechno-zemnoi fizike* (KAPG Simpozium on Solar-Terrestrial Physics). Book of Abstracts 3. Moscow: Nauka Pbl, 72–73.
7. Belyaev PP, Polyakov SV, Rapoport VO, et al. (1989) Theory for the formation of resonance structure in the spectrum of atmospheric electromagnetic background noise in the range of short-period geomagnetic pulsations. *Radiophys Quantum Electron* 32: 594–601.
8. Belyaev PP, Polyakov SV, Rapoport VO, et al. (1990) The ionospheric Alfvén resonator. *J Atmos Terr Phys* 52: 781–788.
9. Trakhtengerts VY, Feldstein AY (1991) Turbulent Alfvén boundary layer in the polar ionosphere. 1. Excitation conditions and energetic. *J Geophys Res Space Phys* 96: 19363–19374.
10. Lysak RL (1991) Feedback instability of the ionospheric resonant cavity. *J Geophys Res Space Phys* 96: 1553–1568.
11. Lysak RL, Yoshikawa A (2006) Resonant cavities and waveguides in the ionosphere and atmosphere. *Magnetospheric ULF Waves.Geophys Monograph Ser V*, Washington DC USA: American Geophysical Union, 289–306.
12. Belyaev PP, Bösinger T, Isaev SV, et al. (1999) First evidence at high latitudes for the ionospheric Alfvén resonator. *J Geophys Res Space Phys* 104: 4305–4317.
13. Yahnin AG, Semenova NV, Ostapenko AA, et al. (2003) Morphology of the spectral resonance structure of the electromagnetic background noise in the range of 0.1–4 Hz at L = 5.2. *Ann Geophys* 21: 779–786.
14. Pokhotelov OA, Feygin FZ, Khabazin Y, et al. (2003) Observations of IAR spectral resonance at a large triangle of geophysical observatories. *Proc XXVI Annual Seminar Apatity: Physics of Auroral Phenomena*. *Kola Science Center RAS*, 123–126.
15. Molchanov OA, Schekotov AY, Fedorov E, et al. (2004) Ionospheric Alfvén resonance at middle latitudes: Results of observations at Kamchatka. *Phys Chem Earth* 29: 649–655.
16. Bösinger T, Haldoupis C, Belyaev PP, et al. (2002) Special properties of the ionospheric Alfvén resonator observed at a low-latitude station (L = 1.3). *J Geophys Res Space Phys* 107: 1281–1289.
17. Potapov AS, Polyushkina TN, Dovbnya BV, et al. (2014) Emissions of ionospheric Alfvén resonator and ionospheric conditions. *J Atmos Sol Terr Phys* 119: 91–101.
18. Potapov AS, Polyushkina TN, Oinats AV, et al. (2015) Adaptation of IRI-2012 model for estimation of IAR harmonic structure. *Proceedings of PIERS 2015*, Prague PIERS, 2012–2016.
19. Potapov AS, Polyushkina TN, Tsegmed B, et al. (2017) Considering the potential of IAR emissions for ionospheric sounding. *J Atmos Sol Terr Phys* 164: 229–234.
20. Baru NA, Koloskov AV, Yampolsky YM, et al. (2016) Multipoint observations of Ionospheric Alfvén Resonance. *Adv Astron Space Phys* 6: 45–49.
21. Demekhov AG, Belyaev PP, Isaev SV, et al. (2000) Modelling the diurnal evolution of the resonance spectral structure of the atmospheric noise background in the Pc1 frequency range. *J Atmos Sol Terr Phys* 62: 257–265.
22. Hebden SR, Robinson TR, Wright DM, et al. (2005) A quantitative analysis of the diurnal evolution of Ionospheric Alfvén resonator magnetic resonance features and calculation of changing IAR parameters. *Ann Geophys* 23: 1711–1721.

23. Parent A, Mann IR, Rae IJ (2010) Effects of substorm dynamics on magnetic signatures of the ionospheric Alfvén resonator. *J Geophys Res Space Phys* 115: A02312.
24. LEMI LLC (2016) LEMI Sensors. Available from: https://lemisensors.com/?p=274/.
25. Balogh A, Hudson HS, Petrovay K, et al. (2015) Introduction to the Solar Activity Cycle: Overview of Causes and Consequences. In: Balogh A, Hudson H, Petrovay K, et al. (eds), *The Solar Activity Cycle. Space Sciences Series of ISSI*. Springer, New York, NY, Vol 53.
26. National Weather Service (2020) Hello Solar Cycle 25. Available from: https://www.weather.gov/news/201509-solar-cycle.
27. Britannica (2020) Dalton minimum. Available from: ttps://www.britannica.com/science/Dalton-minimum/.
28. WDC-SILSO (2020) Royal Observatory of Belgium, Brussels. Available from: http://sidc.oma.be/silso/datafiles/.
29. NASA/Goddard Space Flight Center (2020) Space Physics Data Facility, OMNIWeb. Available from: https://omniweb.gsfc.nasa.gov/ow.html.
30. GFZ German Research Centre for Geosciences (2020) GFZ Data Services. Available from: ftp://ftp.gfz-potsdam.de/pub/home/obs/kp-ap/wdc/.
31. Data Analysis Center for Geomagnetism and Space Magnetism (2020) Graduate School of Science, Kyoto University World Data Center for Geomagnetism. Available from: http://wdc.kugi.kyoto-u.ac.jp/dstae/index.html/.
32. Nosé M, Uyeshima M, Kawai J, et al. (2017) Ionospheric Alfvén resonator observed at low-latitude ground station, Muroto. *J Geophys Res Space Phys* 122: 7240–7255.
33. Fedorov EN, Mazur NG, Pilipenko VA, et al. (2016) Modeling diurnal variations of the IAR parameters. *Acta Geod Geophys* 51: 597–617.
34. Semenova NV, Yahnin AG (2014) Sudden change in the resonance structure in the electromagnetic noise spectrum in the 0.1–10 Hz range during a substorm. *Geomagn Aeron* 54: 316–322.
35. Potapov AS, Polyushkina TN, Oinats AV, et al. (2016) First attempt to estimate the ion content over the ionosphere using data from the IAR frequency structure. *Sovrem Probl Distantsionnogo zondirovaniya Zemli Kosmosa* 13: 192–202.
36. Kunitsyn VE, Nazarenko MO, Nesterov IA, et al. (2015) Solar flare forcing on ionization of upper atmosphere. Comparative study of several major X-class events of 23rd and 24th solar cycles. *Moscow Univ Phys Bull* 70: 312–318.
37. Fedorov E, Mazur N, Pilipenko V, et al. (2016) Modeling the high-latitude ground response to the excitation of the ionospheric MHD modes by atmospheric electric discharge. *J Geophys Res Space Phys* 121: 11282–11301.

AIMS Press